

Article

Graphene Oxide Reinforcing Genipin Crosslinked Chitosan-Gelatin Blend Films

George Mihail Vlasceanu ^{1,2} , Livia Elena Crica ², Andreea Madalina Pandele ^{2,3} and Mariana Ionita ^{1,2,*}

¹ Faculty of Medical Engineering, University Politehnica of Bucharest, Gh Polizu 1-7, 011061 Bucharest, Romania; vlasceanu.georgemihail@yahoo.ro

² Advanced Polymer Materials Group, University Politehnica of Bucharest, Gh Polizu 1-7, 011061 Bucharest, Romania; livia.crica@gmail.com (L.E.C.); pandele.m.a@gmail.com (A.M.P.)

³ Faculty of Applied Chemistry and Materials Sciences, University Politehnica of Bucharest, Gh Polizu 1-7, 011061 Bucharest, Romania

* Correspondence: mariana.ionita@polimi.it; Tel.: +40-21-402-2709

Received: 4 February 2020; Accepted: 21 February 2020; Published: 23 February 2020



Abstract: This study was targeted towards the synthesis and characterization of new chitosan–gelatin biocomposite films reinforced with graphene oxide and crosslinked with genipin. The composites' mode of structuration was characterized by Fourier Transform Infrared spectroscopy and X-ray diffraction, while morphology and topography were investigated by scanning electron microscopy, nano-computer tomography and profilometry. Eventually, thermal stability was evaluated through thermogravimetric analysis, mechanical properties assessment was carried out to detect potential improvements as a result of graphene oxide (GO) addition and in vitro enzyme degradation was performed to discern the most promising formulations for the maturation of the study towards in vivo assays. In accordance with similar works, results indicated the possibility of using GO as an agent for adjusting films' roughness, chemical stability and polymer structuration. The enzymatic stability of chitosan–gelatin (CHT-GEL) films was also improved by genipin (GEN) crosslinking and GO supplementation, with the best results being obtained for CHT-GEL-GEN and CHT-GEL-GEN-GO3 (crosslinked formulation with 3 wt.% GO). Yet, contrary to previous reports, no great enhancement of CHT-GEN-GEL-GO thermal performances was obtained by the incorporation of GO.

Keywords: biopolymer blend; graphene oxide; genipin; composite films; morphostructural characterization

1. Introduction

Biopolymers represent an essential class of biomaterials in continuous development. Blends fabricated out of a wide range of natural or synthetic constituents serve as versatile convertible materials fit to typify assorted conformations such as bulks, films or membranes, as well as porous scaffolds and fibers [1]. When developing new biomaterials, natural polymers are often preferred to other classes of materials, as a result of their higher biocompatibility and similarities to human body constituents. For instance, some of the most popular natural biopolymers are chitosan [2], collagen [3] and gelatin [4], hyaluronic acid [5], sodium alginate [6,7], nanocellulose [8] and silk fibroin [9].

Chitosan (CHT), a natural derivative of chitin [10], gained its notoriety in the biomedical sphere through its great biocompatibility, biodegradability, low cytotoxicity and antimicrobial performances, maturing into one of the most used natural biopolymers worldwide [11]. Gelatin (GEL) is another preeminent biomaterial, originating from collagen, the most abundant protein in the human body, and is the functional and constituent component of connective tissue, muscles and bones [12]. Being less antigenic than its precursor, the prevalence of gelatin in the biomaterial development area has

gradually increased [13]. Lately, numerous studies reported the development of chitosan and gelatin composite systems in the form of sponges, capsules or films, for wound dressing, drug delivery and tissue engineering [14–19]. However, chitosan–gelatin blends often lack proper physico-chemical stability and mechanical strength. Common shortages like this can be lessened through cross-linking or reinforcing treatments.

While glutaraldehyde and CaCl_2 possess remarkable crosslinking capacities, their use decreased with the occurrence of cytotoxic effects. A more reliable and biological-friendly alternative is the use of genipin (GEN), a natural extract of Gardenia fruits that acts as cross-linker for amino groups in biopolymers without toxic side effects [20–22]. The literature-reported data indicate great performances of genipin in both the crosslinking and biological activity of chitosan and gelatin biocomposites [23]. Further, the reinforcement of biopolymers employs reinforcing agents such as silk fibers, ceramic particles and graphene or graphene oxide (GO), which are able to receive, transfer and dissipate mechanical stress more efficiently within the polymer matrix [24,25]. GOs are defined as functionalized sheets of graphene with carboxyl, hydroxyl and epoxide groups on their surface and edges [26]. Numerous studies indicate that GO is a superior fortifier for polymer-based materials, which can impressively enhance mechanical and thermal resistance even at low loadings [27,28]. For chitosan and gelatin porous composites, GO led to higher structural stability for both dry and wet states, by setting electrostatic forces and H bonds between chitosan and GO [2,29,30].

By revising the former results and indications, we pondered upon the development of a composite films system based on a GO-reinforced chitosan–gelatin matrix cross-linked with genipin. Composite materials were synthesized by a simple casting method and characterized thereafter by Fourier-Transform Infrared-Spectroscopy (FTIR), X-Ray Diffraction (XRD), thermogravimetric analysis (TGA), scanning electronic microscopy (SEM), nano-computer tomography (nCT) and profilometry. Additionally, after the depiction of structural and morphological features, mechanical properties and in vitro degradability were also assessed.

2. Materials and Methods

Materials. Graphene oxide, crab shell-derived medium molecular weight chitosan, gelatin from coldwater fish, Genipin ($\geq 98\%$, High Performance Liquid Chromatography (HPLC) grade) and Acetic acid ($\geq 99.7\%$) were purchased from Sigma-Aldrich (St. Louis, MI, USA). All materials were used without additional purification. The water used in this work was double distilled water. Collagenase (lyophilized powder from *Clostridium histolyticum*, ≥ 125 CDU/mg solid), Sodium azide ($\geq 99.5\%$), Calcium chloride ($\geq 97\%$), Tris-HCl, Ethylenediaminetetraacetic acid ($\geq 99\%$) were purchased from Sigma-Aldrich and used without additional purification. Phosphate Buffer Saline (powder, pH 7.4) was used to prepare the aqueous (double distilled water) solution for sample hydration prior to the degradation onset.

Manufacture of CHT-GEL-GEN-GO films. CHT-GEL-GEN-GO samples with GO concentrations of 0.5, 1, 2 and 3 wt.% were prepared and cross-linked by 0.5 wt.% GEN solution. Each formulation was obtained in a volume of 50 mL of polymer by mixing 1 wt.% CHT and 5 wt.% GEL solutions. The weight ratio between dry CHT and GEL was 1:1. The proportion of GEN and GO correspond to the total polymer amount. A total of 41.66 mL of 1 wt.% CHT solution was obtained in 1 wt.% acetic acid (aq) at 50 °C. Adequate GO quantities were weighted and dispersed in 8.33 mL distilled water under sonication conditions for a duration of 1 h. Subsequently, 5 wt.% GEL solution was obtained by dissolving the corresponding amount in the GO aq dispersions. CHT and GEL-GO solutions were then mixed under vigorous stirring for 30 min at room temperature. GEN solution (1 wt.% aq) was added in order to crosslink the CHT-GEL-GEN-GO composites, under the same stirring conditions. The composite solutions and controls were casted in Petri dishes and left undisturbed for the solvent evaporation. The control and composite films that were synthesized were denominated as follows: CHT-GEL for chitosan–gelatin, CHT-GEL-GEN for genipin-crosslinked chitosan–gelatin, CHT-GEL-GEN-GO0.5/1/2/3 for genipin-crosslinked chitosan–gelatin with 0.5, 1, 2 and 3 wt.% GO content.

The GO dispersion procedure was carried out using a VCX 750 ultrasonic device from Sonics & Materials, Inc. (Newton, CT, USA) provided with a Ti-6Al-4V probe tip and a 750 W processor operating at 20 kHz. The amplitude of the probe tip vibrations was set at 70% throughout the 1 h GO exfoliation procedure.

Fourier Transform Infrared Spectroscopy. To investigate the CHT-GEL-GEN-GO interactions, FTIR studies were carried on a SHIMADZU 8900 (Kyoto, Japan) equipment. The FTIR spectra were registered in a 600–4000 cm^{-1} range with a 4 cm^{-1} resolution, as an average of 32 records per sample.

X-Ray Diffraction. To study the crystalline structure and the GO-reinforced composites and controls, X-ray diffraction measurements were done at room temperature using a Panalytical X'Pert Pro MPD (Malvern, UK) instrument provided with a Cu $K\alpha$ radiation source.

Thermogravimetric analysis. The thermal stability of the biopolymer-GO composites was evaluated by means of a Q500 TA Instruments equipment (New Castle, DE, USA), using nitrogen atmosphere from room temperature to 700 °C at a heating rate of 10 °C/min

Scanning Electron Microscopy. The morphological investigations of CHT-GEL-GO composite films and controls were performed by using the QUANTA INSPECT F Scanning Electron Microscope (Waltham, MA, USA).

Nano-Computer Tomography. For the nano-computer tomography analysis, Bruker (Kontich, Belgium) nanoCT 2211 high-resolution equipment was used. The scanning was carried out without a filter, with a source voltage of 45 kV, current intensity of 200 μA and exposure per frame of 300 ms, respectively. The samples were rotated by 180°, with a rotation step of 0.1°. For each individual slice, the image was the result of averaging five frame captures. Throughout the sample set acquisition, the image pixel size corresponded to 3.5 μm . Tomograms were reconstructed from the raw data in Bruker NRecon 1.7.1.6 software, were visualized in Bruker's CTvox, while the profile graphics were transcribed from Bruker's DataViewer.

Profilometry. Profilometry assessments were done by confocal analysis using an optical imaging profiler PL μ 2300 (Terrassa, Spain) with an objective of 50 \times and data were processed using SensoMap 2.0 software.

Mechanical properties. Mechanical behavior of the CHT-GEL and CHT-GO-GEN-GO composite films was studied by testing under tensile stress with a speed of 2 mm/min, by using a universal mechanical tester (Instron, Model 3382, Norwood, MA, USA). A number of 3–4 specimens per sample were tested and each one was 6 cm long and 1 cm wide. The presented results are average values of the measurements.

Enzyme degradation study. The reported enzymatic degradation was based on a previously described method [31]. Briefly, the in vitro enzyme-mediated degradation was carried out by incubating composite specimens of equal size in a 0.5 mL Tris-HCl (0.1 M, pH 7.4) buffer solution supplemented with 0.005% (*w/v*) NaN_3 and 5 mM CaCl_2 for 1 h, followed by the addition of 0.5 mL collagenase solution (200 $\mu\text{g/mL}$). The test was carried out at 37 °C in quadruplicate for each composite formulation and controls, and then averaged. Sample degradation was stopped by collagenase inactivation after 10/20/40/60/120/240 min by the addition of 0.1 mL of 0.25 M ice-cold EDTA solution and accelerated cooling on ice bath. Upon collagenase cutoff, samples were rinsed three times with ice-cold Tris-HCl and three times with ice-cold double distilled water. Gel fraction (GF) was determined after sample-drying in air at 37 °C by employing the following equation

$$\text{GF (\%)} = (W_{d,t}/W_0) \times 100\%,$$

where $W_{d,t}$ is the weight of the dried sample, at time t of degradation, and W_0 is the initial weight of the sample.

3. Results

3.1. Fourier Transform Infrared Spectroscopy

Figure 1 illustrates the recorded FTIR spectra of GO, CHT-GEL, CHT-GEL-GEN and CHT-GEL-GEN-GO with 0.5, 1, 2 and 3 wt.% GO. A typical GO spectrum is defined by the absorption

bands situated around 1050–1060, 1200–1225, 1600–1620 and 1735 cm^{-1} and generated by the vibrational modes of C–O, C–OH, C=C and C=O groups, while –OH functionalities in their both free and connected states are identified, with the band spreading sideways around 3500 cm^{-1} [32–34]. In our case, the above-mentioned absorption bands are placed at 1051, 1212, 1620, 1740, and from 3000 to 3600 cm^{-1} (Figure 1G). Further on, the CHT-GEL FT-IR spectrum comprises the main absorption bands of both CHT and GEL compounds (Figure 1A). At 1025 and 1150 cm^{-1} , respectively, C–O and C–O–C specific marks of CHT are present. Amide I, II and III can be identified at 1654, 1546 and 1249 cm^{-1} , while N–H stretching vibrations in amide A and B are overlapped with the O–H-specific band.

A CHT fingerprint is established within the 900–1155 cm^{-1} region and denotes the stretching vibrations of the glycolide backbone, i.e., C–O–C asymmetric stretching at ~ 1166 and C–O bonds at 1030 cm^{-1} . The bands from 1400 to 1470 indicate the vibrational modes of C–N and N–H that are probably overlapped with the signal of the GEN ring stretching mode structure vibration generated at 1410 cm^{-1} [35,36], while C=O stretching of amide and acetamide bands are positioned at 1647 and 1656 cm^{-1} [37]. The presence of amide B, as well as I, II and III amides of GEL, can be assigned to the absorbance peaks located near 2940 1655, 1546 and 1234 cm^{-1} [38]. Similarly, the –O–H broad band around 3450 cm^{-1} is identified on both CHT and GEL spectra, overlapping the N–H signals in the latter one, whereas C–H symmetric and asymmetric vibration modes are expressed at around 2910 and 2940 cm^{-1} [39]. The GO composites spectra reveal little structural change; nonetheless, the ratio of amide II and amide III equilibrates when GO is added and does not fluctuate with the amount (Figure 1C–F).

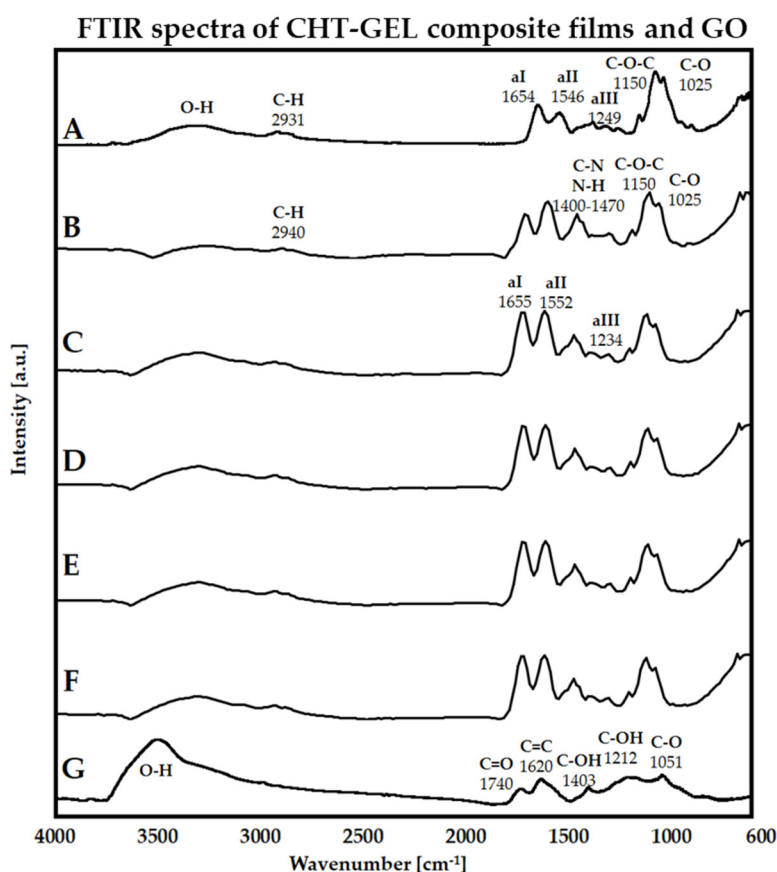


Figure 1. FTIR spectra of CHT-GEL (A), CHT-GEL-GEN (B), CHT-GEL-GEN-GO05 (C), CHT-GEL-GEN-GO1 (D), CHT-GEL-GEN-GO2 (E), CHT-GEL-GEN-GO3 (F), graphene oxide powder (G).

3.2. X-ray Diffraction

The main target of XRD studies was to establish the influence of GO on CHT-GEL composites' general mode of structuration. According to the spectra displayed in Figure 2G, the specific GO-intense peak is generated at $2\theta \sim 10.63^\circ$ and is associated to an interlayer spacing of 0.14 nm. The values obtained for the graphene derivative used in this study are thus clarified to be specific to GO and in accordance to the literature reports [40,41]. The XRD pattern of the unloaded composite (Figure 2A,B) consists of three diffraction peaks located at 8.25° , 11.40° and 17.95° and a broad band at around 23° . The intensity maximums at 8.25° and 17.95° are attributed to the organized and unorganized domains of GEL. Their correspondent d-spacing values of 0.11 and 0.23 nm are in direct relation to the diameter of the triple helical structures and the distance between amino-acid components, respectively [42,43]. The peak identified at 11.40° , as well as the broad band at 23° , are attributed to the semi-crystalline structure of chitosan [44,45].

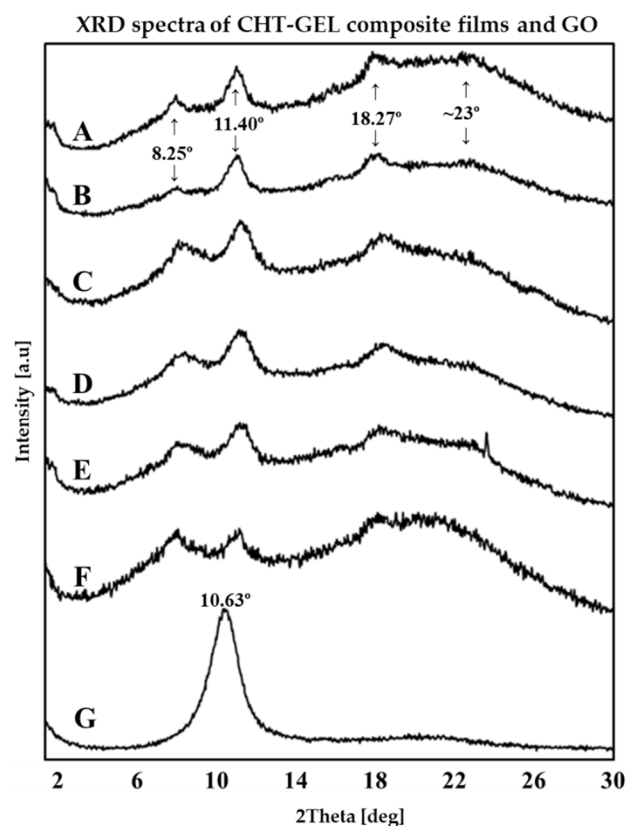


Figure 2. XRD spectra of CHT-GEL (A), CHT-GEL-GEN (B), CHT-GEL-GEN-GO05 (C), CHT-GEL-GEN-GO1 (D), CHT-GEL-GEN-GO2 (E), CHT-GEL-GEN-GO3 (F), graphene oxide powder (G).

3.3. Thermogravimetry (TGA)

During TGA assessments, controls and CHT-GEL-GEN-GO specimens were heated from room temperature to 600°C and the recorded thermograms are illustrated in Figure 3, with correlated numerical data listed in Table 1. Similar to reported TGA studies of both CHT and GEL, our samples' thermal behavior can be described by three distinctive degradation steps [46]. Accordingly, water molecules in both their free and associated states are eliminated during the first phase, while the major polymer degradation takes place during the second phase, when protein and polysaccharide domains are degraded [46]. Eventually, the third step denotes the carbonization of residual compounds.

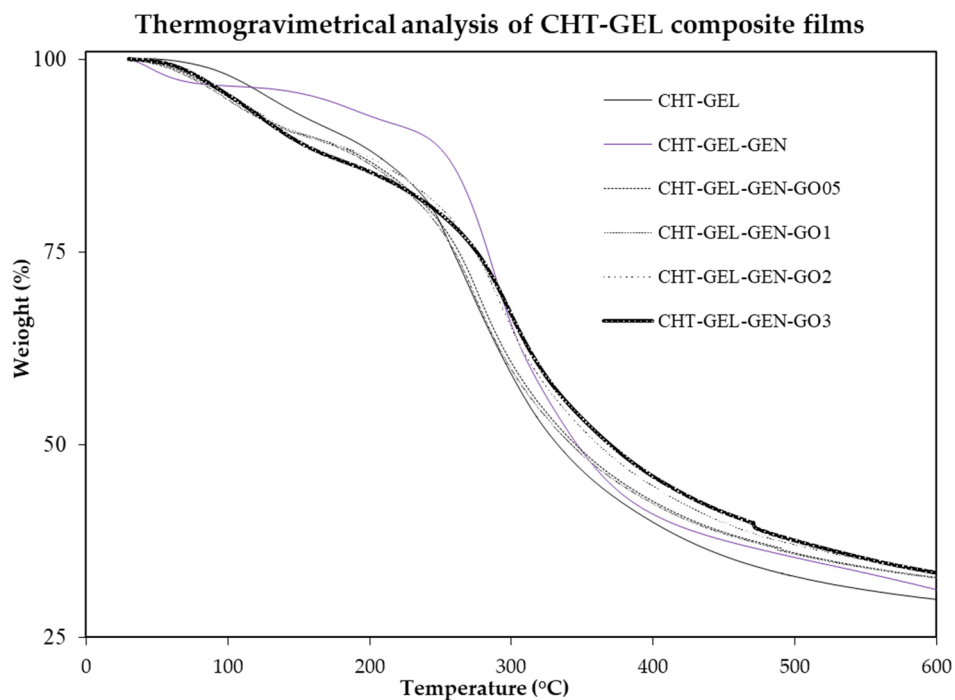


Figure 3. TGA curves obtained for the biopolymer–GO composite films and control.

3.4. Scanning Electron Microscopy

Morphologies of biopolymer–GO composite films were investigated by SEM. In Figure 4, the surfaces of composite films are illustrated. Throughout the image set, the classical features of polymer blend films are present: flat surfaces with no porosity. However, a developmental surface morphology associated with the increase in GO load can be stressed. The superficial appearance of pure polymer blends is gradually changed from smooth to rough upon the increasing GO amount. The surface features of the polymer blend composite films are similar overall. Segregated clusters of insoluble chitosan residues appeared for all formulations. This lack of homogeneity amongst the films' framework could be the result of low amounts of chitosan powder with different degrees of deacetylation.

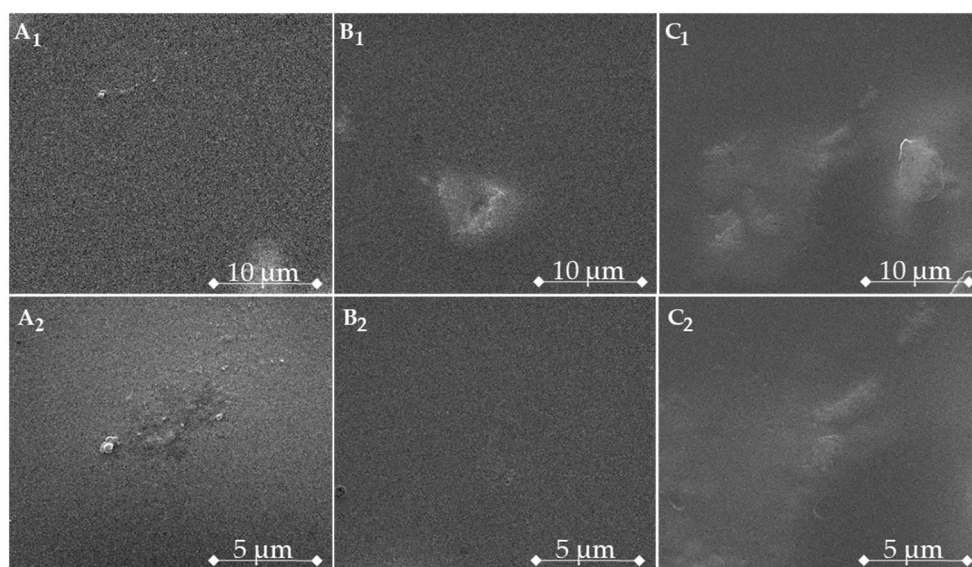


Figure 4. Cont.

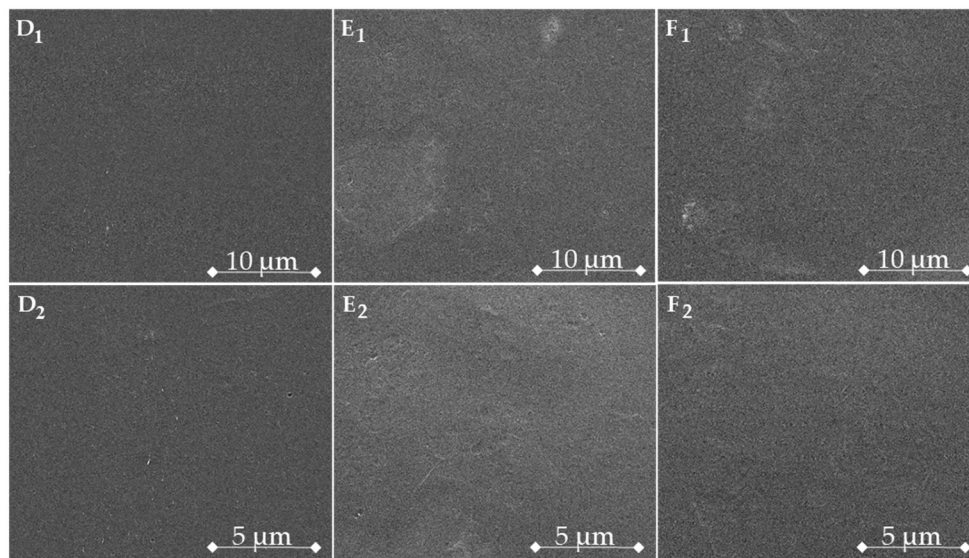


Figure 4. SEM images of CHT-GEL (A1,A2), CHT-GEL-GEN (B1,B2), CHT-GEL-GEN-GO05 (C1,C2), CHT-GEL-GEN-GO1 (D1,D2), CHT-GEL-GEN-GO2 (E1,E2), CHT-GEL-GEN-GO3 (F1,F2) films at two different magnifications (1—10,000 \times , 2—20,000 \times).

3.5. Profilometry

Bearing in mind that the topography and rugosity of a biomaterial play a major role in further biological performances, both control and GO-containing composite films were evaluated by optical profilometry imaging and measurements. All the scanned samples presented smooth surfaces, with rugosity (Ra) values in the nanometric range (Table 2). Prior to the analysis of GO influence on samples Ra, it is interesting to observe the effect of genipin, which, in this case, increased Ra from 86 nm for neat CHT-GEL samples to 184 nm for CHT-GEL-GEN. Subsequently, Ra is markedly decreased to 39 and 52 nm by 0.5 and 1 wt.% GO incorporation. Thereafter, the Ra is increased again to values higher than CHT-GEL, yet lower than CHT-GEL-GEN.

3.6. Nano-Computer Tomography

NanoCT acquisition amassed on the residual specimens of CHT-GEL and composite films after the mechanical assay was performed. Therefore, it was possible to highlight the fracture profiles conforming to the film type, as well as the in-depth survey of the peripheral protrusions identified in micrographies and the profilometry test.

3.7. Mechanical Properties

In order to assess the impact of GO incorporation on composites' mechanical performance, 3–4 equal-sized specimens (6 cm length, 1 cm width) of each formulation underwent tensile tests at a speed of 2 mm/min. Typical stress–strain curves were obtained as the basis for tensile strength and Young's modulus calculation. Tensile strength was directly extracted as the maximum supported tensile stress, while Young's modulus was calculated as the slope of the linear ascending region in the early stages of the characteristic curves. Their corresponding averaged numerical data, with standard deviation, are plotted in Figure 5.

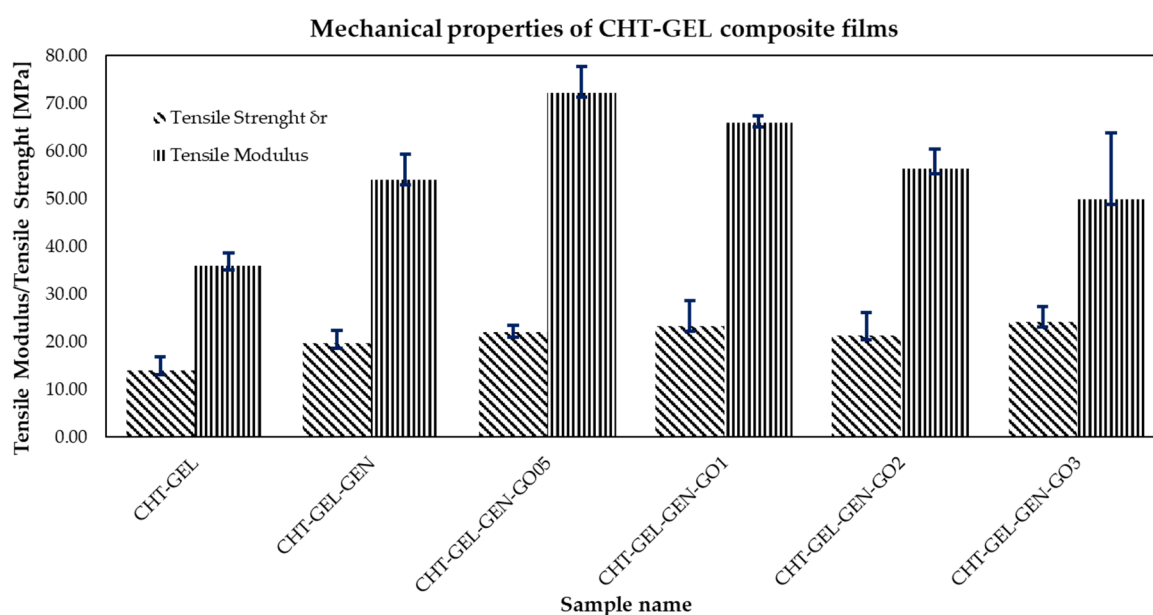


Figure 5. Tensile modulus and tensile strength of CHT-GEL and CHT-GEL-GEN-GO composite films.

3.8. Enzyme Degradation

In order to assess the *in vitro* stability of biopolymer-GO scaffolds, a chemical degradation test was carried out in collagenase-enriched human-simulated medium. Composite films with GO contents of 0.5–2 wt.% feature a quasilinear behavior even at extended degradation times. After 240 min, the measured weight loss is almost 40%, comparable to the materials most susceptible to the enzyme effect, that is, the CHT-GEL control. Upon increasing the GO content to 3 wt.%, a significant improvement of roughly 10% was observed. With respect to time, in less than one hour, CHT-GEL-GEN-GO3 exhibits strong resistance against enzymatic activity.

4. Discussion

Structurally, in FTIR spectra, for the crosslinked control (Figure 1B), the 1400–1470 vibration bands of CH=N are more pronounced as a result of CHI-GEL crosslinking with GEN [47]. Compared with CHT-GEL spectra, in the genipin crosslinked blend, a decrease in the amide II and amide I peaks' ratio appears, as well as a slight shift, to 1654 and 1552 cm^{-1} . This is associated with the susceptibility of the primary amine to react to GEN through nucleophilic attack by the amino group of CHI-GEL and the dihydropyran ring opening. A shift of 1654 cm^{-1} describes post-crosslinking heterocyclic amine generation. In composite formulation, the peak ratio (C–N and C–O stretching vibration) is balanced, indicating that the crosslinker reaction could be slightly impeded by the GO presence. CHI-GEL crosslinking carries through the Schiff base reaction. GO could alter the structuration of CHI within the crosslinked network by the reaction amide groups in chitosan with a carboxyl of GO [48].

FTIR spectra revealed that the progressive addition of GO amounts within the CHT-GEL matrix does not seem to cause other alterations within the samples' spectra, hence no significant increase, decrease or shifts in the typical absorption bands were identified. The lack of GO signals within the composites' spectra could be due to FTIR limitations in detecting both the well-dispersed GO sheets and those in low amounts. Nevertheless, XRD characterization pointed out the fact that once GO sheets are incorporated within composites (Figure 2C–F), a slight sharpening of the maximum at 23°, as well as an increase in intensity for the peak at 11.4°, can be observed, suggesting that GO holds the ability to promote CHT-GEL crystalline features. The absence of a GO-specific intensity maximum from the composites' spectra may support the idea of adequate GO nanosheets' dispersion throughout the material's volume.

The beneficial effect of graphene derivatives' incorporation into the establishment of more ordered polymeric structures, with improved a response towards thermal stimuli and longer-lasting properties, has been long-established [49]. Conversely, the thermal stabilities of our samples tended to decrease with the progressive addition of GO for the early degradation stages, while the situation is reversed from the middle of the process.

As a result, CHT-GEL-GEN-GO samples degrade at lower temperatures than the control samples when temperatures lower than ~300 °C are applied, with values of Td3% decreasing from 110 to 62 °C for the maximum GO incorporation. However, for temperatures greater than 300 °C, less weight loss occurs at the same temperatures in the case of GO-containing composites. Interestingly, GEN crosslinking increases the thermal stability of the blend up to approximately 250 °C (Figure 3), while crosslinking CHT-GEL supplemented with GO does not have the same remarkable performance. On the basis on these results, and while the beneficial versus detrimental effects of GO on polymeric materials are not fully elucidated, supplementary studies should be carried out. However, it is known that GO is an excellent heat conductor that provides a constant and mild energy dissipation throughout the matrix it embeds [50]. All the specimens with a GO load have a slightly lower weight loss at the end of the treatment, while CHT-GEL-GEN-GO05 was the most stable formulation. One of the reasons for this is that low concentrations of GO can adequately disperse within organic matrices and provide a high physico-chemical properties enhancement, as equally scattered GO sheets can restrain polymer catenae mobility.

Table 1. TGA numerical data of Td3% and final weight loss.

Sample	GO Content [wt.%]	Td3% [°C]	Weight Loss [%]
CHT-GEL	0	110.54	70.09
CHT-GEL-GEN	0	72.11	68.93
CHT-GEL-GEN-GO	0.5	70.81	66.11
CHT-GEL-GEN-GO	1	80.25	67.28
CHT-GEL-GEN-GO	2	70.94	66.78
CHT-GEL-GEN-GO	3	62.09	67.47

SEM images of CHI-GEL films reinforced with GO revealed variations in topographical features on the specimen outer and, overall, a commonly smooth surface, specific to polymer non-porous sheets. By visual examination, the polymer blends' roughness seems comparable. However, between the CHT-GEL-GEN (B) and CHT-GEL (A), a minor difference appeared, which could be the consequence of crosslinking. When CHT-GEL gels form, polymer chains are strained and their reorientation is restricted. For that reason, crosslinking induces an additional superficial tension which improves the outer evenness. By comparison, the GO-loaded samples exhibit an interesting tendency related to the surface roughness. The SEM images (C–F) depict a visible gain in the films' surface roughness, varying in agreement with the incrementing carbonaceous material amount. In the case of 2 and 3 wt.% GO-enriched films, the features of superficial roughness mimic typical graphene flake morphology. The films' outer side texture consists of fold-like structures of different sizes which are dispersed graphene sheets covered by the polymer matrix.

All six formulations feature slightly irregular spherical protrusions onto their surface which span from the film bulk. Generally, they are divergently distributed or form loose clusters with no compact agglomerations. It is the opinion of the authors that these textures are micron-range unsolubilized chitosan particles, randomly confined inside the homogeneous composite matrix, and not morphological features associated with the drying step. As evidence, in the reconstructed nanoCT images (Figure 6), these irregularities are displayed in very bright shades of gray and white, an indication of highly compact or dense areas.

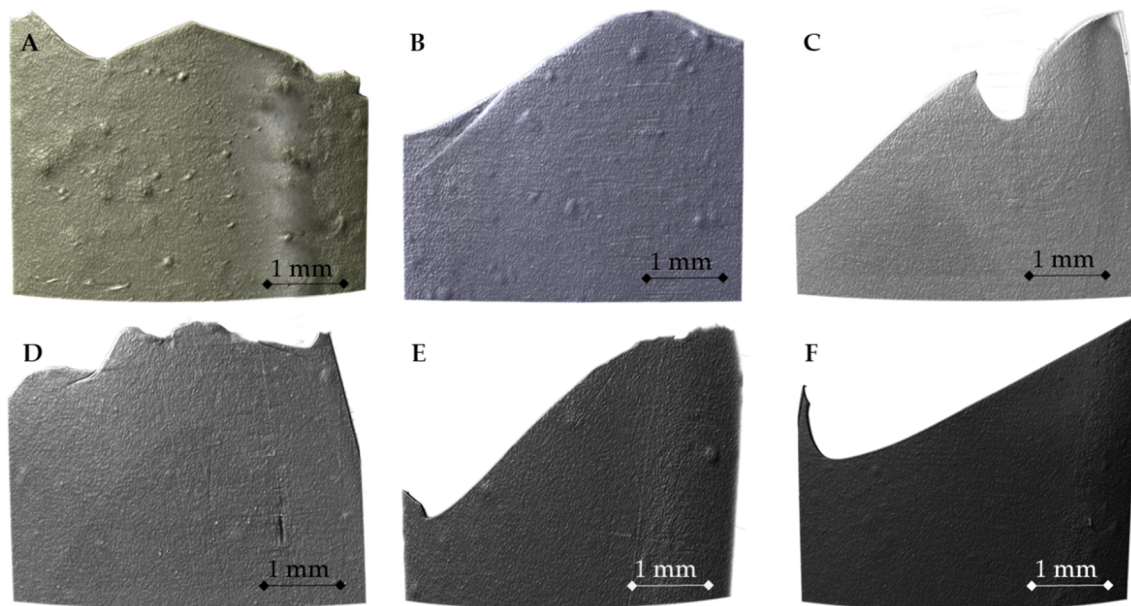


Figure 6. NanoCT images of CHT-GEL (A), CHT-GEL-GEN (B), CHT-GEL-GEN-GO05 (C), CHT-GEL-GEN-GO1 (D), CHT-GEL-GEN-GO2 (E), CHT-GEL-GEN-GO3 (F).

All images are edited with respect to color and contrast and, in particular A, B, D–F are altered in order to focus on the CHT grain distribution among the constituent matrix of the film. Image C was altered for the purpose of highlighting the film-splitting pattern during the tensile test.

Fracture profiles seem to span from very sharp to smooth, according to the sample kind. The CHT-GEL specimen features sharp and clean breaks along the film defects, while the break line of the crosslinked control sample is less sharp and with radial small fissures. The GO-containing films continue the trend of smoother breakpoints with the GO content increment. For the 0.5 and 1 wt.% GO specimens, the fracture profile follows the distribution of the insoluble CHT clusters, though at higher concentrations the splitting is clean and with no apparent positioning in the vicinity of heterogeneous areas.

The GO-specific wrinkled topography was consistent throughout the film surface, to a lower extent in the case of CHT-GEL-GEN-GO05 and CHT-GEL-GEN-GO1. The roughness enhancement with the GO:biopolymer ratio increase is a strong indication that GO has a direct impact on the amassing of superficial protrusions. These observations are in accordance with the profilometry data (Table 2) that suggested a directly proportional relation between the GO content and surface roughness and protrusion magnitude. By regulating CHT-GEL-GEN material topography, GO-loading could improve the biological properties of the polymer blend, as cellular adhesion is augmented on roughened facets.

Materials' topography was evaluated through the analysis of height distribution skewness (Ssk) and results are given in Table 2. By all accounts, a positive value of Ssk indicates the existence of superficial protuberances such as peaks, while a negative value denotes a surface characterized by smooth and profound valleys. Positive values were obtained for all our samples and are consistent with the reconstructed topographies illustrated in Figure 6A,B for CHT-GEL-GEN and CHT-GEL-GEN-GO0.5 wt.%, respectively. The high variance in Ssk-reported values may be due to the sensitivity of the method towards noise. Such profilometry outcomes support the idea that materials' surface topography and roughness can be adjusted by the variation in GO amounts, and thus aided in the development of certain types of materials.

Table 2. Height distribution skewness (Ssk) of composite and control film.

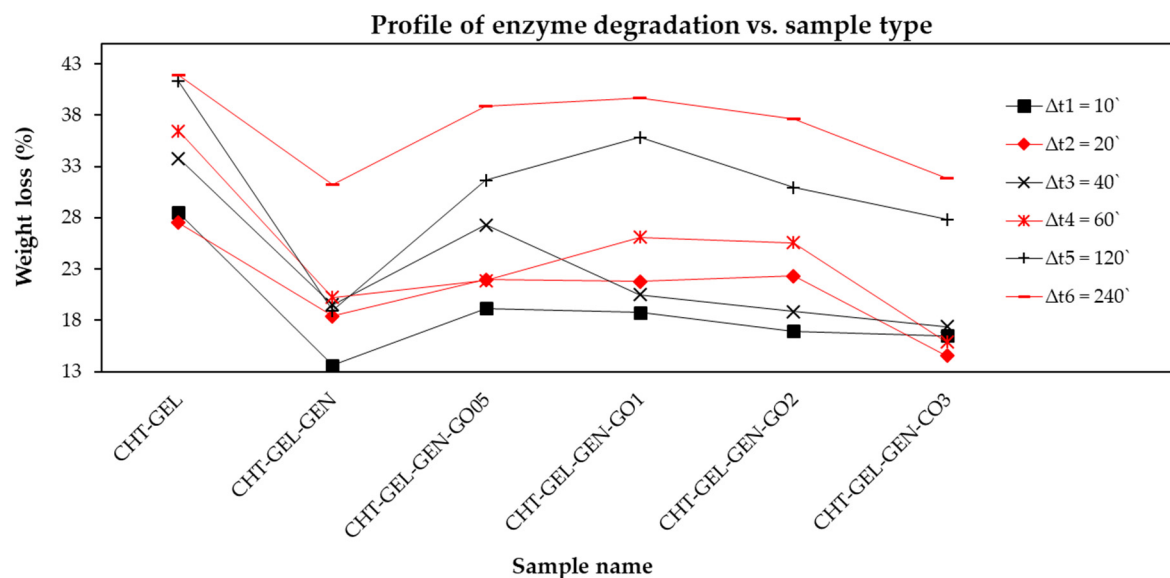
Sample	GO Content [wt.%]	Surface Rugosity [μm]	Ssk
CHT-GEL	0	0.086	0.349
CHT-GEL-GEN	0	0.184	2.706
CHT-GEL-GEN-GO	0.5	0.039	16.050
CHT-GEL-GEN-GO	1	0.052	0.603
CHT-GEL-GEN-GO	2	0.126	0.688
CHT-GEL-GEN-GO	3	0.178	2.175

As a consequence of being subjected to mechanical testing, composites exhibited an improvement in both the Young's modulus and the tensile strength associated to the GO filling. A clear linear increase can be observed for CHT-GEL, CHT-GEL-GEN, CHT-GEL-GEN-GO05. Upon a higher GO addition, Young's modulus fluctuates slightly.

The most favorable composition proves to be that of 0.5 wt.% GO, for which the tensile modulus and tensile strength significantly increase from 19.62 to 21.99 MPa and from 54 to 70.3 MPa, respectively. The decline in tensile modulus values after elevating GO concentration to 1, 2 and 3 wt.% is presumably due to a lesser GO sheet dispersion within the polymer matrix. As a result, load transfer at the biopolymer blend/GO interface is impeded. Nonetheless, an increase in both the tensile strength and Young's modulus, able to surpass the pristine biopolymer effectiveness, was also observed for these composites.

Furthermore, as in the case of thermal features, a slight influence could be attributed to the more ordered structure of composite materials' biopolymer/GO, as indicated by XRD investigation.

In vitro biodegradability was performed as a preliminary assessment of the in vivo behavioral shifts associated to the GO enrichment of the polymer blend. The results are illustrated in Figure 7. For CHT-GEL-GEN-GO formulations and controls, the weigh-loss percentage was plotted against enzymatic reaction length for each material. Firstly, it is difficult to identify a direct correspondence between the sample composition and the weight loss. For short collagenase exposure intervals, the biopolymer-GO compositions exhibit superior chemical stability compared to the CHT-GEL control, but poorer than genipin crosslinked specimens. Overall, the most stable formulation seems to be the crosslinked control, followed by the composite films in a GO-content decreasing succession.

**Figure 7.** Time-dependent enzyme degradation weight loss of the composite films and controls.

GO was reported to improve the biostability of polymeric structures *in vivo* and simulated internal media. Nonetheless, the discrepancy between the composite films' degradation profiles could be the result of occasional GO restacking within the biopolymer matrices. Upon GO addition, the crosslinking of CHT and GEL is altered due two factors: for one, the planar structure of GO partially veils the interface between polymer chains, resulting in a weak crosslinking density. In addition, genipin can tether functional groups from the carbon nanomaterials' surface with other graphenic layers or polymers, generating complex structures with a random map of covalent bonds distribution. Even so, by increasing the graphene fill, enzyme stability tends to improve, due to the fact that extra layers of graphene act as a barrier that better obstructs collagenase–gelatin contiguity.

Hence, the deficient enzymatic stability of CHT-GEL films could be improved by genipin crosslinking and the addition of precise GO content. CHT-GEL-GEN and CHT-GEL-GEN-GO3 are the candidates with the most promising prospects for *in vivo* permanence.

5. Conclusions

Chitosan and gelatin are two of the most important and advantageous biopolymers used in the sphere of biomaterial engineering, with benefits such as biocompatibility, biodegradability, low antigenicity, low cost and processability into various outlines. However, like most biopolymers, their structures often require stabilization and toughening via cross-linking or reinforcement with various agents, especially when in the form of films or 3D porous systems. Nowadays, the majority of scientific reports place genipin on the top of the low-toxic cross-linkers hierarchy, while graphene oxide is considered to be one of the most performant reinforcing agents.

Herein, the synthesis protocol of a biopolymer blend-graphene oxide composite biomaterial is prospected, which the authors anticipate to emerge as a most influential formulation in bone tissue engineering. The novelty of the study resides in purposing two natural polymers with complementary traits in a complex network by means of crosslinking with a nontoxic compound and reinforcement with graphene oxide.

The compositional analysis of the assembly revealed a suitable GO dispersion within the polymer blend, as the carbonaceous nanosheets specific signals lack both FTIR and XRD, and the spectral features of CHT-GEL persisted as the GO load increased. Thermogravimetrically, the composite films experienced accelerated degradation at first, but overall, the weight loss at the end of the process was inverse to the GO proportion.

The image characterization results were paired to fully illustrate the film morphology. The samples present classical rather smooth surfaces, with irregular segregated protuberances extending inside the film volume. On a smaller scale, wrinkle-like topography alterations were distinguished by SEM imaging. In accordance with the reinforcing concentration, a similar impact of GO onto the superficial roughness, a requisite for cell attachment, was found by the profilometry survey.

The polymer blend reinforcement constructively impacted the films Young's modulus and the tensile strength. Improvements were significant in comparison with the controls and upon GO ratio increment. Recorded values followed a descending linear profile due to deficient nanosheets homogenization.

For future extensive *in vivo* investigations, CHT-GEL and composite films could be tuned in terms of collagenase stability by genipin crosslinking and GO loading. CHT-GEL-GEN was the most promising material, while, due to moderate GO dispersion, only CHT-GEL-GEN-GO3 could be comparable with the control with respect to *in vivo* assurance.

Composite films' synthesis can be optimized in terms of improving the GO dispersion within the polymer matrix, without damaging the blend components. At this moment, CHT-GEL-GEN-GO05 and CHT-GEL-GEN-GO3 stand out from a mechanical resistance point of view and for *in vitro* stability, respectively. Still, GO proved it could be an influential reinforcing agent that purposefully tailors biopolymer properties.

Author Contributions: Conceptualization, M.I.; methodology, G.M.V., L.E.C.; investigation, G.M.V., L.E.C. and A.M.P.; data curation, G.M.V. and L.E.C.; writing—original draft preparation, G.M.V. and L.E.C.; writing—review and editing, G.M.V., L.E.C. and M.I.; funding acquisition, M.I. All authors have read and agreed to the published version of the manuscript.

Funding: This work was supported by a grant of the National Authority for Scientific Research and Innovation, Operational Program Competitiveness Axis 1-Section E Program cofinanced from European Regional Development Fund “Investments for Your Future” under Project no. 154/25.11.2016, P_37_221/2015.

Acknowledgments: The Nano Computer Tomography experiments were possible due to European Regional Development Fund through Competitiveness Operational Program 2014-2020, Priority axis 1, ID P_36_611, MySMIS code 107066, INOVABIOMED. G.M.V. acknowledges the support of Operational Programme Human Capital of the Ministry of European Funds through the Financial Agreement 51668/09.07.2019, SMIS code 124705. The authors thank Eugeniu Vasile (University Politehnica of Bucharest) for the valuable contribution in obtaining the scanning electron microscope images of the films addressed in this paper.

Conflicts of Interest: The authors declare no conflict of interest.

References

- Kohane, D.S.; Langer, R. Polymeric biomaterials in tissue engineering. *Pediatr. Res.* **2008**, *63*, 487–491. [[CrossRef](#)] [[PubMed](#)]
- Dinescu, S.; Ionita, M.; Ignat, S.-R.; Costache, M.; Hermenean, A. Graphene oxide enhances chitosan-based 3D scaffold properties for bone tissue engineering. *Int. J. Mol. Sci.* **2019**, *20*, 5077. [[CrossRef](#)] [[PubMed](#)]
- Bherwani, A.; Chang, C.-C.; Pelled, G.; Gazit, Z.; Gazit, D.; Rafailovich, M.; Simon, M. The influence of polymer blends on regulating chondrogenesis. *Coatings* **2019**, *9*, 451. [[CrossRef](#)]
- Dinescu, S.; Ionita, M.; Pandele, A.M.; Galateanu, B.; Iovu, H.; Ardelean, A.; Costache, M.; Hermenean, A. In vitro cytocompatibility evaluation of chitosan/graphene oxide 3D scaffold composites designed for bone tissue engineering. *Biomed. Mater. Eng.* **2014**, *24*, 2249–2256. [[CrossRef](#)]
- Dinescu, S.; Gălăţeanu, B.; Albu, M.; Lungu, A.; Radu, E.; Hermenean, A.; Costache, M. Biocompatibility assessment of novel collagen-sericin scaffolds improved with hyaluronic acid and chondroitin sulfate for cartilage regeneration. *Biomed. Res. Int.* **2013**, *2013*, 598056. [[CrossRef](#)]
- Ionita, M.; Pandele, M.A.; Iovu, H. Sodium alginate/graphene oxide composite films with enhanced thermal and mechanical properties. *Carbohydr. Polym.* **2013**, *94*, 339–344. [[CrossRef](#)]
- Cernencu, A.I.; Lungu, A.; Dragusin, D.; Serafim, A.; Vasile, E.; Ionescu, C.; Iovu, H. Design of cellulose–alginate films using PEG/NaOH aqueous solution as co-solvent. *Cellulose* **2017**, *24*, 4419–4431. [[CrossRef](#)]
- Cernencu, A.I.; Lungu, A.; Stancu, I.-C.; Serafim, A.; Heggset, E.; Syverud, K.; Iovu, H. Bioinspired 3D printable pectin-nanocellulose ink formulations. *Carbohydr. Polym.* **2019**, *220*, 12–21. [[CrossRef](#)]
- Nisal, A.; Sayyad, R.; Dhavale, P.; Khude, B.; Deshpande, R.; Mapare, V.; Shukla, S.; Venugopalan, P. Silk fibroin micro-particle scaffolds with superior compression modulus and slow bioresorption for effective bone regeneration. *Sci. Rep.* **2018**, *8*, 1–10. [[CrossRef](#)]
- Griffith, L. Polymeric biomaterials. *Acta mater.* **2000**, *48*, 263–277. [[CrossRef](#)]
- Rinaudo, M. Chitin and chitosan: Properties and applications. *Prog. Polym. Sci.* **2006**, *31*, 603–632. [[CrossRef](#)]
- Lee, C.H.; Singla, A.; Lee, Y. Biomedical applications of collagen. *Int. J. Pharm.* **2001**, *221*, 1–22. [[CrossRef](#)]
- Alizadeh, M.; Abbasi, F.; Khoshfetrat, A.; Ghaleh, H. Microstructure and characteristic properties of gelatin/chitosan scaffold prepared by a combined freeze-drying/leaching method. *Mater. Sci. Eng. C* **2013**, *33*, 3958–3967. [[CrossRef](#)] [[PubMed](#)]
- Tvl, H.B.; Vidyavathi, M.; Kavitha, K.; Sastry, T.; RV, S.K. Preparation and evaluation of ciprofloxacin loaded chitosan-gelatin composite films for wound healing activity. *Int. J. Drug Deliv.* **2010**, *2*, 173–182.
- Ng, W.L.; Yeong, W.Y.; Naing, M.W. Development of polyelectrolyte chitosan-gelatin hydrogels for skin bioprinting. *Procedia CIRP* **2016**, *49*, 105–112. [[CrossRef](#)]
- Liu, Y.; An, M.; Wang, L.; Qiu, H. Preparation and characterization of chitosan-gelatin/glutaraldehyde scaffolds. *J. Macromol. Sci. B* **2014**, *53*, 309–325. [[CrossRef](#)]
- Roehm, K.D.; Madihally, S.V. Bioprinted chitosan-gelatin thermosensitive hydrogels using an inexpensive 3D printer. *Biofabrication* **2017**, *10*, 015002. [[CrossRef](#)]

18. Azizian, S.; Hadjizadeh, A.; Niknejad, H. Chitosan-gelatin porous scaffold incorporated with Chitosan nanoparticles for growth factor delivery in tissue engineering. *Carbohydr. Polym.* **2018**, *202*, 315–322. [[CrossRef](#)]
19. Qiao, C.; Ma, X.; Zhang, J.; Yao, J. Molecular interactions in gelatin/chitosan composite films. *Food Chem.* **2017**, *235*, 45–50. [[CrossRef](#)]
20. Yoo, J.S.; Kim, Y.J.; Kim, S.H.; Choi, S.H. Study on genipin: A new alternative natural crosslinking agent for fixing heterograft tissue. *Korean J. Thorac. Cardiovasc. Surg.* **2011**, *44*, 197. [[CrossRef](#)]
21. Chen, H.; Ouyang, W.; Lawuyi, B.; Prakash, S. Genipin cross-linked alginate-chitosan microcapsules: Membrane characterization and optimization of cross-linking reaction. *Biomacromolecules* **2006**, *7*, 2091–2098. [[CrossRef](#)] [[PubMed](#)]
22. Wan, C.; Frydrych, M.; Chen, B. Strong and bioactive gelatin–graphene oxide nanocomposites. *Soft Matter* **2011**, *7*, 6159–6166. [[CrossRef](#)]
23. Gorczyca, G.; Tylingo, R.; Szewda, P.; Augustin, E.; Sadowska, M.; Milewski, S. Preparation and characterization of genipin cross-linked porous chitosan–collagen–gelatin scaffolds using chitosan–CO₂ solution. *Carbohydr. Polym.* **2014**, *102*, 901–911. [[CrossRef](#)] [[PubMed](#)]
24. Galli, M.; Fornasiero, E.; Cugnoni, J.; Oyen, M.L. Poroviscoelastic characterization of particle-reinforced gelatin gels using indentation and homogenization. *J. Mech. Behave. Biomed. Mater.* **2011**, *4*, 610–617. [[CrossRef](#)]
25. Kailasanathan, C.; Selvakumar, N. Comparative study of hydroxyapatite/gelatin composites reinforced with bio-inert ceramic particles. *Ceram. Int.* **2012**, *38*, 3569–3582. [[CrossRef](#)]
26. Acik, M.; Chabal, Y.J. Nature of graphene edges: A review. *Jpn. J. Appl. Phys.* **2011**, *50*, 070101.
27. Zhu, Y.; Murali, S.; Cai, W.; Li, X.; Suk, J.W.; Potts, J.R.; Ruoff, R.S. Graphene and graphene oxide: Synthesis, properties, and applications. *Adv. Mater.* **2010**, *22*, 3906–3924. [[CrossRef](#)]
28. Lee, J.J.; Shin, Y.C.; Song, S.-J.; Cha, J.M.; Hong, S.W.; Lim, Y.-J.; Jeong, S.J.; Han, D.-W.; Kim, B. Dicalcium phosphate coated with graphene synergistically increases osteogenic differentiation in vitro. *Coatings* **2018**, *8*, 13. [[CrossRef](#)]
29. Zhang, N.; Qiu, H.; Si, Y.; Wang, W.; Gao, J. Fabrication of highly porous biodegradable monoliths strengthened by graphene oxide and their adsorption of metal ions. *Carbon* **2011**, *49*, 827–837. [[CrossRef](#)]
30. Hermenean, A.; Codreanu, A.; Herman, H.; Balta, C.; Rosu, M.; Mihali, C.V.; Ivan, A.; Dinescu, S.; Ionita, M.; Costache, M. Chitosan-graphene oxide 3D scaffolds as promising tools for bone regeneration in critical-size mouse calvarial defects. *Sci. Rep.* **2017**, *7*, 16641. [[CrossRef](#)]
31. Dragusin, D.-M.; Van Vlierberghe, S.; Dubruel, P.; Dierick, M.; Van Hoorebeke, L.; Declercq, H.A.; Cornelissen, M.M.; Stancu, I.-C. Novel gelatin–PHEMA porous scaffolds for tissue engineering applications. *Soft Matter* **2012**, *8*, 9589–9602. [[CrossRef](#)]
32. de Moraes, A.C.M.; Andrade, P.F.; de Faria, A.F.; Simões, M.B.; Salomão, F.C.C.S.; Barros, E.B.; do Carmo Gonçalves, M.; Alves, O.L. Fabrication of transparent and ultraviolet shielding composite films based on graphene oxide and cellulose acetate. *Carbohydr. Polym.* **2015**, *123*, 217–227. [[CrossRef](#)] [[PubMed](#)]
33. Pant, H.R.; Pokharel, P.; Joshi, M.K.; Adhikari, S.; Kim, H.J.; Park, C.H.; Kim, C.S. Processing and characterization of electrospun graphene oxide/polyurethane composite nanofibers for stent coating. *Chem. Eng. J.* **2015**, *270*, 336–342. [[CrossRef](#)]
34. Yadav, M.; Rhee, K.Y.; Park, S. Synthesis and characterization of graphene oxide/carboxymethylcellulose/alginate composite blend films. *Carbohydr. Polym.* **2014**, *110*, 18–25. [[CrossRef](#)]
35. Butler, M.F.; Ng, Y.-F.; Pudney, P.D.A. Mechanism and kinetics of the crosslinking reaction between biopolymers containing primary amine groups and genipin. *J. Polym. Sci. A Polym. Chem.* **2003**, *41*, 3941–3953. [[CrossRef](#)]
36. Chiono, V.; Pulieri, E.; Vozzi, G.; Ciardelli, G.; Ahluwalia, A.; Giusti, P. Genipin-crosslinked chitosan/gelatin blends for biomedical applications. *J. Mater. Sci. Mater. Med.* **2008**, *19*, 889–898. [[CrossRef](#)]
37. Xu, M.; Wei, L.; Xiao, Y.; Bi, H.; Yang, H.; Du, Y. Molecular structural properties of extracted gelatin from Yak skin as analysed based on molecular weight. *Int. J. Food Prop.* **2017**, *20*, S543–S555. [[CrossRef](#)]
38. Sahoo, R.; Sahoo, S.; Nayak, P.L. Synthesis and characterization of gelatin–chitosan nanocomposite to explore the possible use as drug delivery vehicle. *Eur. Sci. J.* **2013**, *9*, 134–141.

39. Bayer, T.; Bishop, S.; Nishihara, M.; Sasaki, K.; Lyth, S.M. Characterization of a graphene oxide membrane fuel cell. *J. Power Sources* **2014**, *272*, 239–247. [[CrossRef](#)]
40. Toh, S.Y.; Loh, K.S.; Kamarudin, S.K.; Daud, W.R.W. Graphene production via electrochemical reduction of graphene oxide: Synthesis and characterisation. *Chem. Eng. J.* **2014**, *251*, 422–434. [[CrossRef](#)]
41. Liu, F.; Antoniou, J.; Li, Y.; Ma, J.; Zhong, F. Effect of sodium acetate and drying temperature on physicochemical and thermomechanical properties of gelatin films. *Food Hydrocoll.* **2015**, *45*, 140–149. [[CrossRef](#)]
42. Benbettaieb, N.; Karbowiak, T.; Brachais, C.-H.; Debeaufort, F. Impact of electron beam irradiation on fish gelatin film properties. *Food Chem.* **2016**, *195*, 11–18. [[CrossRef](#)] [[PubMed](#)]
43. Youssef, A.M.; Abou-Youcef, H.; El-Sayed, S.M.; Kamel, S. Mechanical and antibacterial properties of novel high performance chitosan/nanocomposite films. *Int. J. Biol. Macromol.* **2015**, *76*, 25–32. [[CrossRef](#)] [[PubMed](#)]
44. Li, Z.; Yang, F.; Yang, R. Synthesis and characterization of chitosan derivatives with dual-antibacterial functional groups. *Int. J. Biol. Macromol.* **2015**, *75*, 378–387. [[CrossRef](#)] [[PubMed](#)]
45. Ahmad, M.; Hani, N.M.; Nirmal, N.P.; Fazial, F.F.; Mohtar, N.F.; Romli, S.R. Optical and thermo-mechanical properties of composite films based on fish gelatin/rice flour fabricated by casting technique. *Prog. Org. Coat.* **2015**, *84*, 115–127. [[CrossRef](#)]
46. Nguyen, T.H.; Lee, B.-T. Fabrication and characterization of cross-linked gelatin electro-spun nano-fibers. *J. Biomed. Sci. Eng.* **2010**, *3*, 1117–1124. [[CrossRef](#)]
47. Gong, Y.; Yu, Y.; Kang, H.; Chen, X.; Liu, H.; Zhang, Y.; Sun, Y.; Song, H. Synthesis and Characterization of Graphene Oxide/Chitosan Composite Aerogels with High Mechanical Performance. *Polymers (Basel)* **2019**, *11*, 777. [[CrossRef](#)]
48. Li, S.; Kong, L.; Wang, H.; Xu, H.; Li, J.; Shi, H. Thermal performance and shape-stabilization of comb-like polymeric phase change materials enhanced by octadecylamine-functionalized graphene oxide. *Energy Convers. Manag.* **2018**, *168*, 119–127. [[CrossRef](#)]
49. Ionita, M.; Pandele, A.M.; Crica, L.; Pilan, L. Improving the thermal and mechanical properties of polysulfone by incorporation of graphene oxide. *Compos. B Eng.* **2014**, *59*, 133–139. [[CrossRef](#)]
50. Hoy, C.F.O.; Naguib, H.E.; Paul, N. Fabrication and control of CT number through polymeric composites based on coronary plaque CT phantom applications. *J. Med. Imaging (Bellingham)* **2016**, *3*, 016001. [[CrossRef](#)]



© 2020 by the authors. Licensee MDPI, Basel, Switzerland. This article is an open access article distributed under the terms and conditions of the Creative Commons Attribution (CC BY) license (<http://creativecommons.org/licenses/by/4.0/>).